Dehydration of chlorite explains anomalously high electrical conductivity in the mantle wedges

Geeth Manthilake, Nathalie Bolfan-Casanova, Davide Novella, Mainak Mookherjee, Denis Andrault

ELECTRICAL CONDUCTIVITY

Dehydration of chlorite explains anomalously high electrical conductivity in the mantle wedges

10.1126/sciadv.1501631

Geeth Manthilake,[1]* Nathalie Bolfan-Casanova,[1] Davide Novella,[1†] Mainak Mookherjee,[2] Denis Andrault[1]

Mantle wedge regions in subduction zone settings show anomalously high electrical conductivity (~1 S/m) that has often been attributed to the presence of aqueous fluids released by slab dehydration. Laboratory-based measurements of the electrical conductivity of hydrous phases and aqueous fluids are significantly lower and cannot readily explain the geophysically observed anomalously high electrical conductivity. The released aqueous fluid also rehydrates the mantle wedge and stabilizes a suite of hydrous phases, including serpentine and chlorite. In this present study, we have measured the electrical conductivity of a natural chlorite at pressures and temperatures relevant for the subduction zone setting. In our experiment, we observe two distinct conductivity enhancements when chlorite is heated to temperatures beyond its thermodynamic stability field. The initial increase in electrical conductivity to ~3 × 10^{-3} S/m can be attributed to chlorite dehydration and the release of aqueous fluids. This is followed by a unique, subsequent enhancement of electrical conductivity of up to 7 × 10^{-1} S/m. This is related to the growth of an interconnected network of a highly conductive and chemically impure magnetite mineral phase. Thus, the dehydration of chlorite and associated processes are likely to be crucial in explaining the anomalously high electrical conductivity observed in mantle wedges. Chlorite dehydration in the mantle wedge provides an additional source of aqueous fluid above the slab and could also be responsible for the fixed depth (120 ± 40 km) of melting at the top of the subducting slab beneath the subduction-related volcanic arc front.

INTRODUCTION

The high electrical conductivity (EC) of up to 1 S/m observed in mantle wedge regions between depths of 40 and 100 km is often attributed to the aqueous fluid released from the descending slab (*1*–*10*). It is well known that mantle silicate minerals are electrical insulators with large electronic band gaps of around 7.5 to 9.5 eV at room temperature (*11*). Owing to the greater mobility of charged ions in a fluid or melt, they are better candidates for explaining the EC that is orders of magnitude greater than the solid silicate mineral phases (*12*).

Laboratory-based measurements of the EC of aqueous fluids at pressure and temperature conditions relevant to the mantle wedge are crucial for explaining these geophysically observed high electrical conductivities (*1*–*10*). Recent studies indicate that at depths greater than 150 km, aqueous fluids are likely to be highly conductive due to the ionization of water molecules to proton (H^+) and hydroxyls (OH^-) (*13*). However, at relatively shallower depths (40 to 100 km), dehydration-induced aqueous fluids are less conductive (<2 × 10^{-2} S/m) (*14*, *15*). Recent estimates based on molecular dynamics simulations (*16*) indicate that a high EC can be explained with fluid salinity of at least 4 to 7 wt %. However, laboratory-based EC measurements of saline fluid–bearing systems (*17*, *18*) indicate that fluid salinity of about 10 wt % is required to explain the high conductivity of up to 1 S/m. Thus, it is difficult to establish a causal relation between the dehydration-induced aqueous fluids and the anomalously high EC of >1 S/m at the shallow wedge mantle without invoking unusually high salinity (>4 wt %), which may account for the high EC observed in certain subduction zone settings (*1*, *5*, *8*–*10*). However, the mechanism responsible for generating saline fluids at shallow mantle conditions is yet to be fully understood.

Dehydration of the subducted hydrous phases and subsequent release of fluids lead to rehydration of the mantle wedge lying above the subducted slab. Chlorite, $(Mg,Fe)_5Al(Si_3Al)O_{10}(OH)_8$, is a major hydrous phase produced in the hydrated peridotite mantle wedge (*19*–*21*). Phase relations in hydrated peridotite indicate that 16% chlorite could be stable at high pressures (<4 GPa) and temperatures (<1100 K), corresponding to a mantle depth of ~120 km (*22*, *23*). Because chlorite contains 13 wt % of H_2O locked as hydroxyl groups (OH^-) into its crystal structure, it can account for 2 to 3 wt % of water in hydrated peridotite (*23*). Despite being a major host of water in the subducting slab and mantle wedge, the EC of chlorite and its dehydration products remains unknown.

RESULTS AND DISCUSSION

Our results indicate that the EC of chlorite is similar to other hydrous silicate minerals (*14*, *15*, *18*). The EC has a weak or no pressure dependence, but varies significantly with temperature. A typical value of EC at 4 GPa and 923 K is 2 × 10^{-4} S/m (Fig. 1). At temperatures greater than 923 K, the EC increases sharply by an order of magnitude to 3 × 10^{-3} S/m. A subsequent increase in EC of more than two orders of magnitude to 7 × 10^{-1} S/m occurred when the sample was held at the same pressure and temperature conditions for a duration of 30 to 40 min (Fig. 1). The EC remained mostly unchanged during the cooling path, back to room temperature.

The sharp increase in EC at around 923 to 973 K coincides with the dehydration of chlorite to olivine, pyrope-rich garnet, magnetite (spinel), and aqueous fluid (*24*) (table S1). Owing to the complete wetting of grain boundaries by the aqueous fluid phase at high pressure and temperature (θ < 60°), the aqueous fluid is likely to develop

[1]Laboratoire Magmas et Volcans, CNRS UMR 6524, Université Blaise Pascal, Institut de Recherche pour le Développement, 63178 Clermont-Ferrand, France. [2]Earth, Ocean, and Atmospheric Sciences, Florida State University, Tallahassee, FL 32306, USA.
*Corresponding author. Email: g.manthilake@opgc.univ-bpclermont.fr
†Present address: Lawrence Livermore National Laboratory, Livermore, CA 94550, USA.

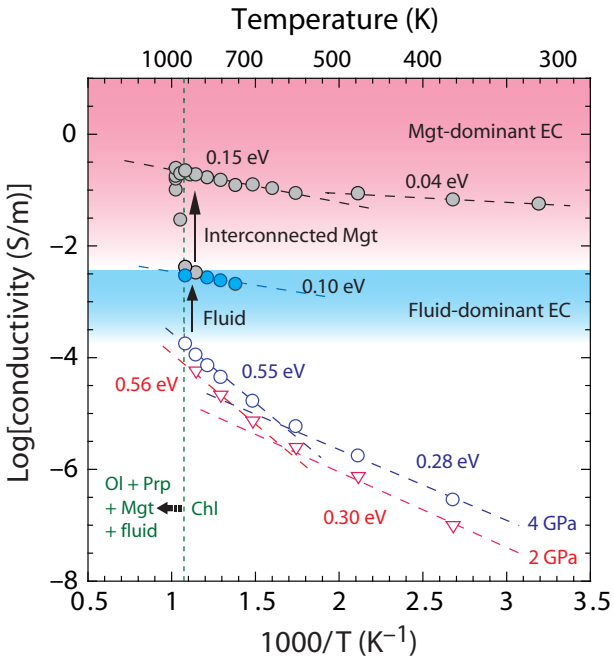

Fig. 1. Plot of the logarithm of EC of chlorite as a function of reciprocal temperature. The inverted triangles and circles refer to data at 2 and 4 GPa, respectively. The first stage of the heating cycle indicates low electrical conductivities (red inverted triangles and blue circles). Upon heating to ~923 K at 4 GPa, that is, beyond the thermodynamic stability field of chlorite (Chl), a discontinuous enhancement of EC by more than one order of magnitude is observed (blue filled circles). A subsequent enhancement of EC by more than two orders of magnitude (gray circles) is also observed after the sample is kept at 923 K. Activation enthalpies are reported in eV, next to the individual fits. The uncertainties in the estimation of the EC result from the estimations of temperature, pressure, sample dimensions, and data-fitting errors and are less than 5%. The green dashed vertical line indicates the thermal stability of chlorite. Mgt, magnetite; Ol, olivine; Prp, pyrope.

an interconnected network all along the grain boundaries (*13*). This fluid network is expected to enhance the EC of the bulk sample, consisting of dehydrated solid mineral assemblages and aqueous fluid. This explains the sharp increase in EC at temperatures >923 K.

Upon chlorite decomposition, iron is partitioned into the dehydrated mineral phases, including olivine and garnet (table S1). In addition, iron also stabilizes magnetite (Fe_3O_4) in the spinel crystal structure. The magnetite phase occurs mainly as grains with acicular or bladed crystal habits, with most of the crystals preferentially oriented along the foliation planes of relict chlorite (Fig. 2). Mineral assemblages examined using electron microprobe analysis (table S1) revealed up to 21% Al^{3+} and Mg^{2+} substitutions for Fe in magnetite, yielding a chemically impure magnetite with $[(Fe_{1.8}Al_{0.2})(Fe_{0.3}Mg_{0.7})O_4]$ stoichiometry. Voids in the recovered sample indicate the presence of aqueous fluids at high pressures and temperatures, which were subsequently lost during the quenching process. The presence of NiO in the electrodes located near the contact with the dehydrated sample indicates an oxygen fugacity close to the Ni-NiO buffer, which compares favorably with the ΔQFM (quartz-fayalite-magnetite) = +0.5 to +2 observed for subduction zone–related arc magmas (*25*, *26*).

On the basis of the microstructural analysis, the significant enhancement of EC by more than two orders of magnitude, following the dehydration of chlorite, could be attributed to the formation of an interconnected network of magnetite grains. Although nucleation and grain growth are time-dependent processes (*27*), formation of magnetite in the presence of aqueous fluids could proceed through rapid agglomeration of nanoparticles, forming three-dimensional clusters (*28*, *29*). The observed time delay of 30 to 40 min between the enhancement of EC due to the aqueous fluid and the subsequent enhancement of EC due to the formation of interconnected chemically impure magnetite grains could be rationalized in terms of the fast kinetics of the magnetite grain growth.

The activation enthalpy (ΔH) provides valuable insight into the conduction mechanisms operating within the sample (table S2). The observed weak dependence of EC as a function of inverse temperature

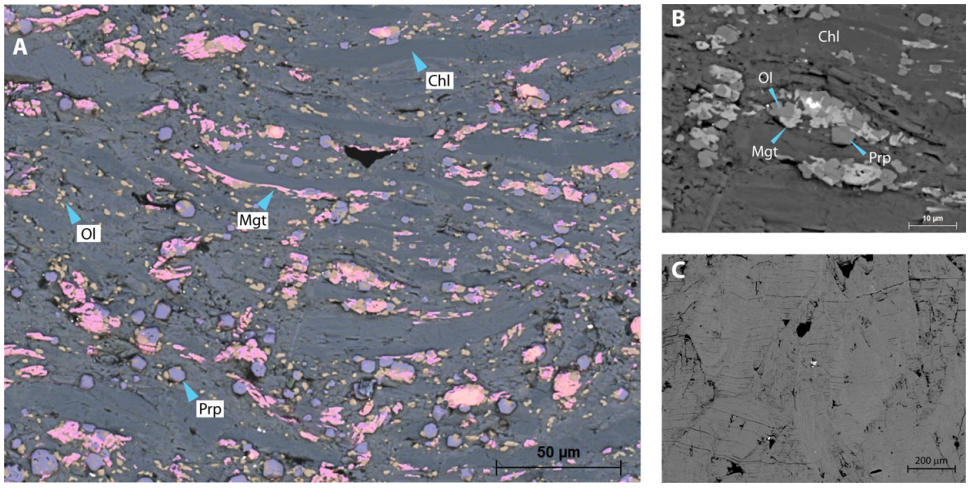

Fig. 2. Electron backscattered images of the recovered samples after the EC measurements. (**A**) Recomposed colored map of the chemical composition of the recovered sample after dehydration at 4 GPa and 973 K. The presence of aqueous fluid in the sample at high pressure and temperature is suggested by the presence of voids (darker regions). The magnetite grains along relict chlorite foliation planes and fracture lines are denoted by white and purple. (**B**) The close-up view of the mineral assemblage of olivine, pyrope, and magnetite is formed by dehydration of chlorite. (**C**) Backscattered electron image of the chlorite sample before the experiments.

leads to a low activation enthalpy of 0.10 (±0.05) eV along the cooling path, following the dehydration of chlorite, and indicates the presence of an interconnected network of aqueous fluids within the bulk sample (blue-shaded area in Fig. 1). The low activation enthalpy of 0.15 (±0.1) eV along the cooling path, following the formation of the interconnected network of oriented magnetite grains (pink-shaded area in Fig. 1), is comparable with the activation enthalpy observed for magnetite in previous studies (*30*, *31*). The temperature-dependent variation in the activation enthalpy along the cooling path, that is, 0.15 (±0.1) eV at high temperatures and 0.04 (±0.01) eV at lower temperatures, is also characteristic of the metallic conduction in magnetite, where additional energy is required at high temperatures to compensate for the electron scattering in metal oxides due to thermal vibrations.

Our experimental measurements demonstrate that the development of an interconnected network of chemically impure magnetite during dehydration of chlorite could explain the anomalously high conductivity observed in the mantle wedge (Fig. 3). Our experimental study demonstrates that aqueous fluids alone cannot explain the anomalously high EC. We note that the serpentinization of peridotite is also associated with the formation of magnetite. However, in previous experiments on EC of serpentine (*14*, *18*), the magnetite grains were reported to occur as isolated grains, and as a result, the mineral assemblages displayed a rather weak bulk EC of ~10^{-4} S/m. Previous EC measurements performed during shear deformation on iron-free serpentine with varying magnetite contents suggest that for magnetite to become an effective conductive medium, a threshold value of 25 volume % is necessary (*32*). However, in our experimental study, a modal abundance of magnetite of only 13.6 ± 2 volume %, formed in situ during the dehydration of chlorite and oriented along the relict chlorite foliations (Fig. 2), contributes to an enhanced interconnectivity and a major change in EC. It is important to note that the Al^{+3} and Mg^{+2} substitutions for Fe induce a significant reduction in the EC of magnetite (*30*). The modeling of EC of magnetite in our sample indicates that 14 volume % magnetite can account for the highest EC of 1 S/m observed in subduction systems (Fig. 3). It is well known that the presence of melt is likely to enhance EC (*33*, *34*); however, because of the low temperatures (<973 K) expected at the shallow mantle wedge region, melting can be ruled out as a possible factor influencing the high EC.

In the mantle wedge, chlorite dehydration could be triggered by the downward drag of the mantle by the corner flows (*35*) and provide an additional source of aqueous fluid for arc melting above the slab (Fig. 4). This could explain why melts produced in arc volcanic fronts appear to be compatible with mantle sources located at a fixed depth of 120 ± 40 km (*36*), a value compatible with the depth of chlorite dehydration in the mantle wedge. As chlorite dehydrates, the aqueous fluid dominates the EC ~2×10^{-4} to 3×10^{-3} S/m. A higher EC of ~7×10^{-1} S/m is produced by the formation of a complete interconnected

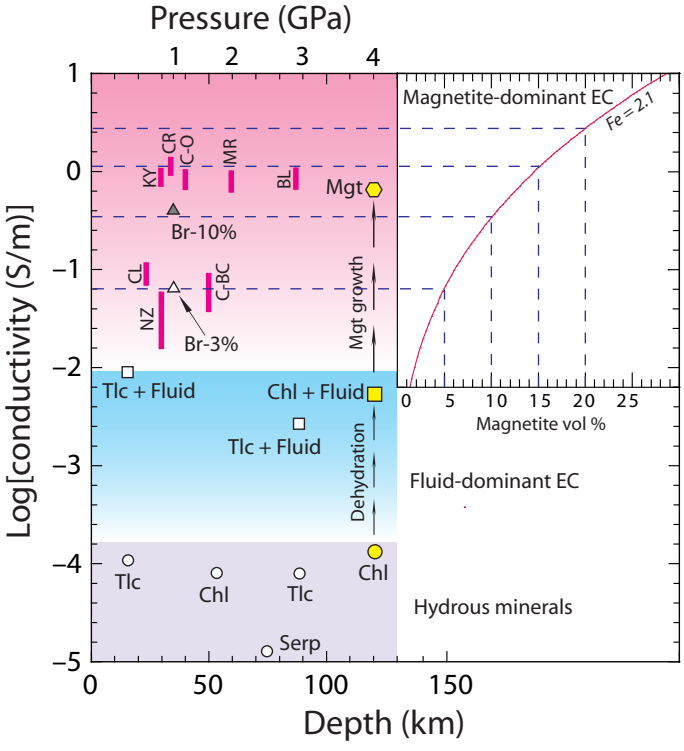

Fig. 3. Magnetotelluric data reported for a variety of subduction zones (pink vertical lines) compared with the range of possible values of EC related to the chlorite dehydration. The shaded purple, blue, and pink regions indicate EC dominated by hydrous minerals, aqueous fluid, and interconnected magnetite, respectively. The conductivity of talc (Tlc) (*14*, *15*), serpentine (Serp) (*11*), dehydrating fluids (*14*, *15*), and brine with 3 and 10 wt % of NaCl (*17*) is also shown for comparison. The red line in the embedded figure (in the upper right corner) indicates the EC of magnetite observed in our sample as a function of magnetite volume fractions (see fig. S1 for details of the calculations). The blue dashed lines indicate the volume fractions of magnetite required to explain the EC of various subduction systems. The magnetotelluric models presented in the figure are Bolivia (BL) (*5*), Cascadia–British Columbia (C-BC) (*2*), Chile (CL) (*6*), Cascadia-Oregon (C-O) (*8*), Costa Rica (CR) (*10*), Kyushu (KY) (*1*), Mariana (MR) (*9*), and New Zealand (NZ) (*7*).

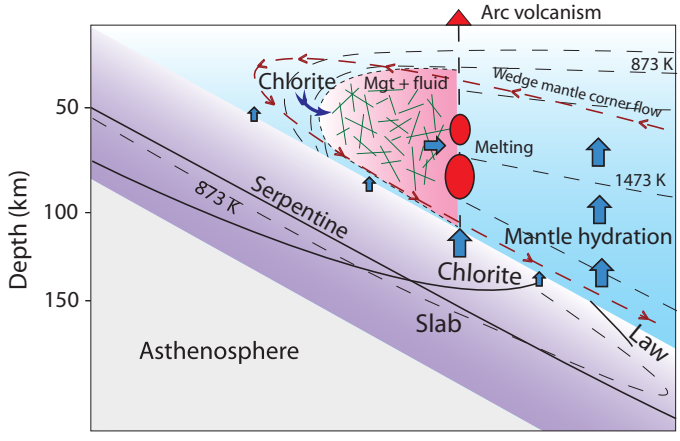

Fig. 4. Geodynamical model explaining the origin of the high-conductivity region in the shallow mantle wedge. First, dehydration of hydrous minerals such as serpentine in the subducting slab generates aqueous fluid. The aqueous fluid leads to rehydration of the mantle wedge and formation of a hydrous phase such as serpentine and chlorite. These mineral phases in the mantle wedge are dragged by corner flows, where chlorite undergoes dehydration when it crosses the wedge mantle isotherm at about 923 K. The dehydration of chlorite leads to the formation of an interconnected network of magnetite grains, which, in turn, explains the very high conductivity measured geophysically. Finally, the dehydration produces a secondary fluid, inducing mantle melting, which creates arc volcanoes, with mantle sources located at a fixed depth of 120 ± 40 km (*36*).

network of chemically impure magnetite grains. The anomalously high EC-based magnetotelluric observation for various subduction zone settings can be well explained by the subtle variations in the aqueous fluid fraction, the volume fractions, and orientation of the chemically impure magnetite grains.

MATERIALS AND METHODS

Sample characterization

Here, we measured the EC of a natural chlorite with $(Mg_{3.77}Fe_{1.23})Al(Si_3Al)O_{10}(OH)_8$ stoichiometry at conditions relevant to the mantle wedge and subduction zone settings. The natural chlorite sample used in this study was from the Ambatomainty region in Madagascar. Before the measurements, the chemical composition was determined by electron probe microanalysis using a JEOL JXA-8200 electron microprobe operating at an accelerating voltage of 15 kV and a beam current of 20 nA. After each experiment, cross sections of run products were investigated using an electron probe microanalyzer and energy-dispersive x-ray spectroscopy (EDS) chemical mapping using a JEOL JSM-5910LV scanning electron microscope.

High pressure–high temperature experiments

We explored two distinct pressures of 2 and 4 GPa and a range of temperatures of up to 973 K using a 1500-ton Kawai-type multianvil apparatus installed at the Laboratoire Magmas et Volcans. The experiments were performed in an 18/11 assembly, with a Cr_2O_3-doped MgO octahedral pressure medium with 18-mm edge length and 11-mm tungsten carbide (WC) anvil truncation. Cylindrical core samples with a diameter of 2 mm and a length of 2.5 mm were placed in a hexagonal boron nitride (hBN) capsule, which electrically insulated the sample from the furnace during the measurements. The high-purity hBN, sintered at a higher temperature and pressure without a binder (BNHP-FINAL Advanced Materials), ensured that there were no B_2O_3-forming reactions with the aqueous fluids. Two Ni discs placed at the top and bottom of the sample served as electrodes for the EC measurements. The presence of Ni was expected to maintain the oxygen fugacity of the sample close to the Ni-NiO buffer. A $W_{95}Re_5$-$W_{74}Re_{26}$ thermocouple junction was placed at one side of the sample, which monitored the temperature. One cable formed the thermocouple, and a separate $W_{95}Re_5$ cable placed at the opposite side of the sample connected to the impedance spectroscope for the EC measurements. MgO ceramic sleeves insulated the electrode wires from the furnace. All ceramic assembly parts, including the pressure medium, were baked at 1000°C for more than 12 hours and stored at 175°C in vacuum furnaces before use.

EC measurements

EC measurements were conducted using impedance spectroscopy method using ModuLab MTS Impedance/Gain-Phase Analyzer in the frequency range of 10^6 to 10^1 Hz. Insulation resistance of the assembly under similar pressure-temperature conditions was determined before the actual experiments. During the experiments, samples were kept at 500 K for more than 12 hours at the desired pressure. While maintaining a temperature of 500 K, electrical resistance of the sample was measured at regular intervals until the sample resistance reached a steady value, often one to two orders of magnitude higher than the resistance measured at the beginning of the heating cycle. This crucial step ensures the removal of the absorbed moisture in the sample capsule and the surrounding area that could otherwise interfere with the measurements at higher temperatures (*37*). Sample resistance was usually measured in several heating-cooling cycles at temperature steps of 50 to 100 K until the heating and cooling paths were reproducible. This minimizes the uncertainty of EC measurements.

The upper temperature limit for each heating cycle was predetermined, considering the stability of chlorite at relevant pressures. This procedure avoids the dehydration during initial heating-cooling cycles. Once the EC of the chlorite samples was established, the temperature was gradually increased to initiate the dehydration, and measurements were performed in smaller temperature steps (25 K). Once the conductivity of the dehydrated sample had been established, the temperature was gradually brought down to room temperature in 25- to 50-K temperature steps while collecting the impedance spectra at each step.

Polycrystalline samples are characterized by a combination of resister-capacitor/constant phase element circuits, and the resistance can be obtained by fitting the impedance spectra to appropriate equivalent circuits. Once the sample resistance has been determined, conductivity can be calculated using the sample diameter and length measured after each experiment, assuming that the sample geometry remained unchanged during the experiment.

The activation enthalpy (ΔH) of each conduction mechanism can be obtained by fitting the data to the Arrhenius equation

$$\sigma = \sigma_0 \exp\left(\frac{-\Delta H}{kT}\right) \quad (1)$$

where σ is the EC (S/m), T is the absolute temperature, σ_0 is the pre-exponential factor (S/m), and k is the Boltzmann constant (J/K). The low activation enthalpy (0.3 eV) below 573 K is likely to result from an extrinsic mechanism, such as the presence of free protons (adsorbed moisture), which had not been removed during the dehydration of the assembly at 573 K. As the temperature increased, intrinsic conduction mechanisms, such as electron hopping between Fe^{+2} and Fe^{+3} (0.55 eV), started to dominate, masking the contribution from free protons.

SUPPLEMENTARY MATERIALS

Supplementary material for this article is available at http://advances.sciencemag.org/cgi/content/full/2/5/e1501631/DC1

fig. S1. EC as a function of volume fraction of magnetite in chlorites.
fig. S2. Electron backscattered images of the nickel (Ni) electrodes after the EC measurements.
fig. S3. Impedance spectra of the sample at different stages of heating.
table S1. The chemical composition of chlorite and its dehydration products.
table S2. The fitting parameters for chlorite, aqueous fluid, and magnetite.
References (*38*, *39*)

REFERENCES AND NOTES

1. M. Ichiki, N. Sumitomo, T. Kagiyama, Resistivity structure of high-angle subduction zone in the southern Kyushu district, southwestern Japan. *Earth Planets Space* **52**, 539–548 (2000).
2. W. Soyer, M. Unsworth, Deep electrical structure of the northern Cascadia (British Columbia, Canada) subduction zone: Implications for the distribution of fluids. *Geology* **34**, 53–56 (2006).
3. S. Yamaguchi, M. Uyeshima, H. Murakami, S. Sutoh, D. Tanigawa, T. Ogawa, N. Oshiman, R. Yoshimura, K. Aizawa, I. Shiozaki, T. Kasaya, Modification of the network-MT method and its first application in imaging the deep conductivity structure beneath the Kii Peninsula, southwestern Japan. *Earth Planets Space* **61**, 957–971 (2009).

4. R. S. McGary, R. L. Evans, P. E. Wannamaker, J. Elsenbeck, S. Rondenay, Pathway from subducting slab to surface for melt and fluids beneath Mount Rainier. *Nature* **511**, 338–340 (2014).
5. H. Brasse, D. Eydam, Electrical conductivity beneath the Bolivian Orocline and its relation to subduction processes at the South American continental margin. *J. Geophys. Res.* **113**, 1–14 (2008).
6. H. Brasse, P. Lezaeta, V. Rath, K. Schwalenberg, W. Soyer, V. Haak, The Bolivian Altiplano conductivity anomaly. *J. Geophys. Res.* **107** EPM 4-1–EPM 4-14 (2002).
7. P. E. Wannamaker, T. G. Caldwell, G. R. Jiracek, V. Maris, G. J. Hill, Y. Ogawa, H. M. Bibby, S. L. Bennie, W. Heise, Fluid and deformation regime of an advancing subduction system at Marlborough, New Zealand. *Nature* **460**, 733–736 (2009).
8. R. L. Evans, P. E. Wannamaker, R. S. McGary, J. Elsenbeck, Electrical structure of the central Cascadia subduction zone: The EMSLAB Lincoln Line revisited. *Earth Planet. Sci. Lett.* **402**, 265–274 (2014).
9. T. Matsuno, N. Seama, R. L. Evans, A. D. Chave, K. Baba, A. White, T.-n. Goto, G. Heinson, G. Boren, A. Yoneda, H. Utada, Upper mantle electrical resistivity structure beneath the central Mariana subduction system. *Geochem. Geophys. Geosy.* **11**, 1–24 (2010).
10. H. Brasse, G. Kapinos, L. Mütschard, G. E. Alvarado, T. Worzewski, M. Jegen, Deep electrical resistivity structure of northwestern Costa Rica. *Geophys. Res. Lett.* **36**, L02310 (2009).
11. U Nitsan, T. J. Shankland, Optical properties and electronic structure of mantle silicates. *Geophys. J. Int.* **45**, 59–87 (1976).
12. T. J. Shankland, M. E. Ander, Electrical conductivity, temperatures, and fluids in the lower crust. *J. Geophys. Res.* **88**, 9475–9484 (1983).
13. G. Manthilake, M. Mookherjee, N. Bolfan-casanova, D. Andrault, Electrical conductivity of lawsonite and dehydrating fluids at high pressures and temperatures. *Geophys. Res. Lett.* **42**, 7398–7405 (2015).
14. X. Guo, T. Yoshino, I. Katayama, Electrical conductivity anisotropy of deformed talc rocks and serpentinites at 3GPa. *Phys. Earth Planet. In.* **188**, 69–81 (2011).
15. D. Wang, S.-i. Karato, Electrical conductivity of talc aggregates at 0.5 GPa: Influence of dehydration. *Phys. Chem. Miner.* **40**, 11–17 (2013).
16. H. Sakuma, M. Ichiki, Electrical conductivity of NaCl-H_2O fluid in the crust. *J. Geophys. Res.* **121**, 577–594 (2016).
17. A. Shimojuku, T. Yoshino, D. Yamazaki, Electrical conductivity of brine-bearing quartzite at 1 GPa: Implications for fluid content and salinity of the crust. *Earth Planets Space* **66**, 2 (2014).
18. B. Reynard, K. Mibe, B. Van de Moortèle, Electrical conductivity of the serpentinised mantle and fluid flow in subduction zones. *Earth Planet. Sci. Lett.* **307**, 387–394 (2011).
19. M. W. Schmidt, S. Poli, Experimentally based water budgets for dehydrating slabs and consequences for arc magma generation. *Earth Planet. Sci. Lett.* **163**, 361–379 (1998).
20. Y. Tatsumi, Migration of fluid phases and genesis of basalt magmas in subduction zones. *J. Geophys. Res.* **94**, 4697–4707 (1989).
21. T. L. Grove, C. B. Till, M. J. Krawczynski, The role of H_2O in subduction zone magmatism. *Annu. Rev. Earth Planet. Sci.* **40**, 413–439 (2012).
22. B. R. Hacker, G. A. Abers, S. M. Peacock, Subduction factory 1. Theoretical mineralogy, densities, seismic wave speeds, and H_2O contents. *J. Geophys. Res.* **108**, 1–26 (2003).
23. T. L. Grove, N. Chatterjee, S. W. Parman, E. Médard, The influence of H_2O on mantle wedge melting. *Earth Planet. Sci. Lett.* **249**, 74–89 (2006).
24. H. Staudigel, W. Schreyer, The Upper thermal stability of clinochlore , Mg_5Al $[AlSi_3O_{10}](OH)_8$, at 10–35 kb P_{H_2O}. *Contrib. Mineral. Petr.* **61**, 187–198 (1977).
25. C. Ballhaus, Redox states of lithospheric and asthenospheric upper mantle. *Contrib. Mineral. Petr.* **114**, 331–348 (1993).
26. M. N. Brounce, K. A. Kelley, E. Cottrell, Variations in $Fe^{3+}/\sum Fe$ of Mariana arc basalts and mantle wedge fO_2. *J. Petrol.* **55**, 2513–2536 (2014).
27. D. Kashchiev, *Nucleation* (Butterworth-Heinemann, Burlington, MA, 2000).
28. J. Baumgartner, A. Dey, P. H. H. Bomans, C. Le Coadou, P. Fratzl, N. A. J. M. Sommerdijk, D. Faivre, Nucleation and growth of magnetite from solution. *Nat. Mater.* **12**, 310–314 (2013).
29. J. Ge, Y. Hu, M. Biasini, W. P. Beyermann, Y. Yin, Superparamagnetic magnetite colloidal nanocrystal clusters. *Angew. Chemie Int. Ed.* **46**, 4342–4345 (2007).
30. A. V. Kovalevsky, A. A. Yaremchenko, E. N. Naumovich, N. M. Ferreira, S. M. Mikhalev, F. M. Costa, J. R. Frade, Redox stability and high-temperature electrical conductivity of magnesium- and aluminium-substituted magnetite. *J. Eur. Ceram. Soc.* **33**, 2751–2760 (2013).
31. E. R. Morris, Q. Williams, Electrical resistivity of Fe_3O_4 to 48 GPa: Compression-induced changes in electron hopping at mantle pressures. *J. Geophys. Res.* **102**, 18139–18148 (1997).
32. S. Kawano, T. Yoshino, I. Katayama, Electrical conductivity of magnetite-bearing serpentinite during shear deformation. *Geophys. Res. Lett.* **39**, 1–5 (2012).
33. T. Yoshino, M. Laumonier, E. McIsaac, T. Katsura, Electrical conductivity of basaltic and carbonatite melt-bearing peridotites at high pressures: Implications for melt distribution and melt fraction in the upper mantle. *Earth Planet. Sci. Lett.* **295**, 593–602 (2010).
34. F. Gaillard, M. Malki, G. Iacono-Marziano, M. Pichavant, B. Scaillet, Carbonatite melts and electrical conductivity in the asthenosphere. *Science* **322**, 1363–1365 (2008).
35. C. B. Till, T. L. Grove, A. C. Withers, The beginnings of hydrous mantle wedge melting. *Contrib. Mineral. Petr.* **163**, 669–688 (2012).
36. Y. Tatsumi, S. Eggins, *Subduction Zone Magmatism* (Blackwell, Oxford, 1995).
37. M. A. G. M. Manthilake, T. Matsuzaki, T. Yoshino, S. Yamashita, E. Ito, T. Katsura, Electrical conductivity of wadsleyite as a function of temperature and water content. *Phys. Earth Planet. In.* **174**, 10–18 (2009).
38. Z. Hashin, S. Shtrikman, A variational approach to the theory of the elastic behaviour of multiphase materials. *J. Mech. Phys. Solids*, **11**, 127–140 (1963).
39. T. Watanabe, K. Kurita, The relationship between electrical conductivity and melt fraction in a partially molten simple system: Archie's law behavior. *Phys. Earth Planet. In.* **78**, 9–17 (1993).

Acknowledgments: We thank J. M. Henot, J. L. Devidal, and A. Mathieu for assistance with the scanning electron microscope, electron microprobe, and EC measurements, respectively. T. Katsura made helpful comments on the manuscript. We thank two anonymous reviewers for their constructive reviews that benefitted the manuscript. **Funding:** G.M. acknowledges funding from the French PNP (Programme National de Planetologie) program [INSU (Institut national des sciences de l'univers)–CNRS] and Actions initiatives OPGC (Observatoire de Physique du Globe de Clermont-Ferrand) 2014. M.M. is currently funded by U.S. National Science Foundation (NSF) award nos. 1634422 and 1639552. N.B.-C. is supported by ANR-11-JS56-01501, and D.A. is supported by ANR-13-BS06-0008. This research was financed by the French Government Laboratory of Excellence initiative n°ANR-10-LABX-0006, the Région Auvergne, and the European Regional Development Fund (Laboratory of Excellence ClerVolc contribution no. 199). **Author contributions:** G.M. designed the experiments, performed the EC measurements, and analyzed the data. G.M., D.N., N.B.-C., and D.A. performed the chemical analyses of the samples. M.M. contributed to the discussion. G.M., M.M., and D.A. wrote the manuscript. All authors participated in the discussion and agreed on the content. **Competing interests:** The authors declare that they have no competing interests. **Data and materials availability:** All data needed to evaluate the conclusions in the paper are present in the paper and/or the Supplementary Materials. Additional data related to this paper may be requested from the authors. All data, analysis details, and material recipes presented in this work are available upon request to G.M.

Submitted 12 November 2015
Accepted 5 April 2016
Published 6 May 2016
10.1126/sciadv.1501631

Citation: G. Manthilake, N. Bolfan-Casanova, D. Novella, M. Mookherjee, D. Andrault, Dehydration of chlorite explains anomalously high electrical conductivity in the mantle wedges. *Sci. Adv.* **2**, e1501631 (2016).

Dehydration of chlorite explains anomalously high electrical conductivity in the mantle wedges

Geeth Manthilake, Nathalie Bolfan-Casanova, Davide Novella, Mainak Mookherjee and Denis Andrault

Sci Adv **2** (5), e1501631.
DOI: 10.1126/sciadv.1501631